

Simulating 2D Waves Propagation in Elastic Solid Media Using Wavelet Based Adaptive Method

H. Yousefi · A. Noorzad · J. Farjoodi

Received: 26 November 2007 / Revised: 14 September 2009 / Accepted: 15 September 2009 /
Published online: 29 September 2009
© Springer Science+Business Media, LLC 2009

Abstract In this study, an improved wavelet-based adaptive-grid method is presented for solving the second order hyperbolic Partial Differential Equations (PDEs) for describing the waves propagation in elastic solid media. In this method, the multiresolution adaptive threshold-based approach is incorporated with smoothing splines as denoiser of spurious oscillations. This smoothing method is fast, stable, less sensitive to noise, and directly applicable to unequally sampled data. However, the conventional methods can not be directly applied to estimate the smoothing parameters; therefore the optimum ranges are captured through trial-and-error efforts. Here, the spatial derivatives are directly calculated in a non-uniform grid by Fornberg fast method. The derivatives are calculated in 2D simulations, applying antisymmetric end padding method to minimize Gibb's phenomenon, caused by the edge effects. Therefore, stable moving front is achieved. In the realistic source modeling, time dependent thresholding method, introduced here, is an efficient and cost effective adaptive scheme as well. Furthermore, level-dependent thresholding scheme is used to diminish the effects of non-physical long period waves reflected by absorbing boundaries. Finally, several 2D finite, infinite and semi-infinite numerical examples are simulated. These examples have fixed, free and absorbing boundary conditions. Here, the robustness of proposed method is demonstrated.

Keywords Interpolating wavelet · Adaptive · Hyperbolic PDEs · Smoothing splines · Anti-symmetric end padding · Level-dependent thresholding · Time-dependent thresholding

H. Yousefi (✉) · A. Noorzad · J. Farjoodi
School of Civil Engineering, College of Engineering, University of Tehran, P.O. Box 11365-4563,
Tehran, Iran
e-mail: hyousefi@ut.ac.ir

H. Yousefi
e-mail: hyg_te@yahoo.com

A. Noorzad
e-mail: noorzad@ut.ac.ir

J. Farjoodi
e-mail: jfarjood@ut.ac.ir

1 Introduction

Adaptive wavelet grid-based methods (and collocation schemes) were successfully applied in elliptic and parabolic PDEs analyses by Cruze [6, 7, 30, 31], Liu et al. [22], Jameson [16, 17], Vaseline et al. [2, 19, 36–38] and Bertoluzza and Castro [3]. Regarding mentioned efforts, in general, wavelets are carried out as a tool to trace high gradient moving fronts.

The present study is to improve multiresolution-based adaptive-grid method for solving the second order hyperbolic PDEs arisen from elastodynamic. However, unlike elliptic and parabolic PDEs, in hyperbolic systems no inherent dissipation is detected [11]. Therefore, even marginal errors can cause erroneous adapted grid points. In the numerical solutions of hyperbolic PDEs, small spurious oscillations (errors) are developed even in simple cases with smooth initial conditions. In the elastic wave modeling, these errors especially are found at the crest of sharp waves or where the waves propagated outwards. In general, these errors are of two categories: (1) the spatial discretization; e.g. the errors resulting from finite difference approximation; (2) the temporal discretization errors due to time integration. These errors are particularly amplified near high gradient zones (with smooth solutions) or semi-singular regions (e.g. representation of seismic sources).

Several adaptive wavelet based schemes have been developed to solve hyperbolic PDEs. Holmström and Waldén [14] developed a wavelet Galerkin method, proper for PDEs with constant coefficients, using orthonormal Daubechies wavelets. Cai and Wang [4] introduced a collocation method in which the derivatives are calculated in the wavelet space. Holmström [13] proposed an interpolating wavelet collocation method in which all calculations are carried out in the physical space. However, in this method the fine scale features might be missed [13].

There are two approaches for controlling spurious oscillations in hyperbolic PDEs solution: (1) reducing the spurious oscillations by post processing solutions, e.g. using low-pass filtering method [11]; (2) adapting locally the order of approximation for controlling Gibb's phenomenon, e.g. using various orders of finite difference scheme [9]. The first approach is applied in this research as it is more applicable and simpler than the second one.

In this regard, smoothing splines (low pass filtering method) have several important advantages in comparison with other smoothing methods. The advantages of smoothing spline of degree $2m - 1$ are: (1) the boundary values are properly estimated [23]. (2) The noises are removed directly from irregularly spaced data; in such cases the standard filtering techniques, used in time series analyses, are awkward [23, 24]. (3) All derivatives are continuous up to $(2m - 2)$ th [27, 28, 34]. (4) The j th derivative ($j \leq k$) converges to $f^{(j)}$, the function f belongs to Sobolev spaces (W_2^k where $k \leq m$). This convergence increases in accordance with the number of sampled points and interpolating property. Moreover, the error bounds remain even if the f is subjected to some random noises [26]. (5) Fast algorithms are developed [15, 34]. (6) Many types of ill-posed problems, regarding data irregularities, are easily handled due to the regularization term [34]. However, the proper selection of the smoothing parameter in this method should be reviewed.

In most ordinary methods, over-smoothing [15] or under-smoothing [20] are due to the selection of smoothing parameters. Herein, a trial-and-error method is used to obtain optimum range of the smoothing parameter and consequently a proper adaptive grid and solution.

The basis of proposed scheme is to approximate spatial derivatives directly in the irregular grid points. For this purpose the fast and recursive Lagrange polynomials, introduced by Fornberg, is used [10]. Anti-symmetric end padding method is used to reduce edge effects from the derivatives in 2D simulations. In this method, the second derivatives are zero

at end points, like in the relaxed cubic spline one [29]. Therefore, the moving fronts are propagated with constant speed. By end padding a signal, the centered difference formulas, causing less fluctuation than one-sided relations, are used to calculate the derivatives at the edge points. Semi-discretized PDEs in spatial domain are solved in time by an explicit integration method (for example 4th Runge-Kutta scheme). The grid points are adapted by Dubuc-Deslauriers (D-D) interpolating wavelet [24, 32], and the noises are diminished by smoothing splines. As all calculations are done in the physical domain, the proposed method is simple and conceptually straightforward.

In the realistic simulations, besides the importance of solution accuracy, the economy and rapidity are also considered. A source simulation is assumed in which the force function increases gradually at source point from zero to maximum value. In this case, if a threshold of very small value is used at the first time steps to obtain an accurate solution, then many unnecessary grid points are obtained during simulation. In case of using the threshold of large value, the calculation speed increases but the accuracy decreases. Here, in Example 3, the time-dependent thresholds are used to have a fast and accurate solution.

Another method, level-dependent thresholding, is also used for numerical simulation. In this method, it is assumed that the threshold is noise level dependent and also pertinent to the signal characteristics which may change at different levels [18]. This method is used here to reduce the effects of non-physical long period waves reflected from absorbing boundaries.

This paper is composed of: Sect. 2, the main concept explanation of multiresolution-based grid adaptation by interpolating wavelets; Sect. 3, the wavelet-based adaptive-grid method for PDEs solution and the spatial derivatives calculations; Sect. 4, the issues related to smoothing splines with uniform weight coefficients; Sect. 5, the examples. The conclusion of this research is presented at the end of the paper.

2 Multiresolution-Based Grid Adaptation

In wavelet theory context, the complete multiresolution property, fast algorithms and data compression ability [24] make wavelets appealing for the numerical solution of PDEs. In multiresolution analysis, each wavelet coefficient (detail or scale) is linked to a particular point of underlying grid. This distinctive property is incorporated with compression power of the wavelets and therefore a uniform grid can be adapted by grid reduction technique. In this method a simple criteria is applied in 1D grid, based on the magnitude of corresponding wavelet coefficients. The existing odd grid points at level j should be removed if their corresponding detail coefficients are smaller than predefined threshold (ε); wavelet coefficients and grid points have one-to-one correspondence [7]. The above mentioned reduction technique can easily be extended to 2D grid points. In this research, the scheme explained in [31] is implemented for 2D grids adaptation. This technique can be improved by using level-dependent thresholding scheme [18] in which various pre-defined thresholds can be regarded for different levels. The developed thresholding method may improve the numerical simulations. Here, Dubuc-Deslauriers (D-D) interpolating wavelets, auto-correlation of Daubechies scaling functions [24], are used for grid adaptation. The boundary wavelets, introduced by Donoho [8], are used in the vicinity of edge points in case of finite grid points.

3 Wavelet-Based Adaptive-Grid Method for Solving PDEs

At the time step ($t = t_n$), if the solution of PDE is $f(x, t)$, then the procedure for PDE solution in adaptive wavelet-based framework is followed as:

1. Determining the grids, adapted by adaptive wavelet transform, using $f(x, t_{n-1})$ (step $n - 1$). The values of points without $f(x, t_{n-1})$, are obtained by smoothing spline fitting method (Sect. 4).
2. Computing the spatial derivatives in the adapted grid using anti-symmetric end padding method (Sect. 3.1).
3. Discretizing PDEs in spatial domain and then solving semi-discrete systems which are discrete in space and continuous in time. To solve ODEs at the time $t = t_n$, the standard time-stepping methods such as Runge-Kutta schemes can be used.
4. Denoising the spurious oscillations directly performed in non-uniform grid by smoothing splines (Sect. 4).
5. Recurring the steps from the beginning.

In practice, the grid is not adapted at each time step regarding computation time. In fact, it is adapted after several time steps (e.g. 10–20 steps) based on the velocity of moving fronts. These moving fronts are captured by adding some extra points to the fronts of adapted grid at each level of resolution (e.g. 2 points to each end at a level).

3.1 Fast Computation of the Spatial Derivatives

The values of spatial derivatives in the grid of the solution, needed in PDEs solution, are achieved by local Lagrange interpolation method. Fornberg fast and recursive method [10] is applied to calculate effectively the derivative coefficients of order k (c_i^k). The coefficients, c_i^k , are defined as follows:

$$\left. \frac{d^k f}{dx^k} \right|_{x=z} \approx \sum_{i=0}^n c_i^k f(x_i). \quad (3.1)$$

The Fornberg method advantage is that the derivative coefficients depend only on the grid points (x_i); therefore, the re-computing of weights is needed only in case of adapted grid changing. The details of Fornberg method are found in [10] where a FORTRAN subroutine is developed for computing the above mentioned weights.

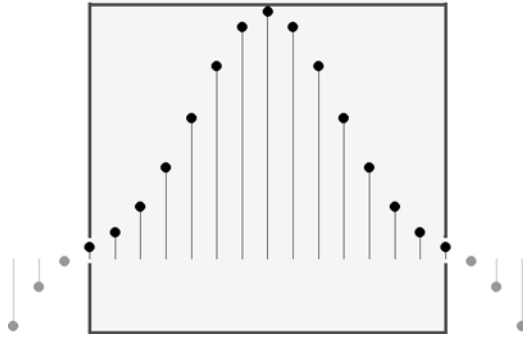
Here, five points are locally chosen to calculate derivatives ($n = 4$ in (3.1)); therefore, a high-order numerical scheme is achieved [16, 17]. In general, higher-order polynomials should be used to obtain higher-order schemes. On the other hand, increasing the order of polynomials, leads to excessive oscillation (Gibb's phenomena). Typically, the 4th order Lagrange interpolation is the proper choice and more economic in comparison with the higher orders.

Practically, the edge effect problems are appeared because of finite length sampled data. These edge effects are handled by extending (end padding) the original signal using several methods, such as zero-padding, symmetric padding, and periodic padding [25].

In this study, smooth padding (extrapolation using splines) and anti-symmetric padding methods are considered as the proper choices. The latter method is applied here as it is cheaper in comparison with the former one.

As the signals are extended, the centered difference formula can be used for all sampled points, x_i ($i = 0, 1, \dots, k$). In fact, the error terms of one-sided derivatives make more fluctuations in the solutions in comparison with centered difference formula. Therefore, in two dimensional analyses, the adapted grid fronts jump locally and not move gradually due to the Gibb's phenomenon. The anti-symmetric end padding of a Gaussian curve is shown in Fig. 1, the light lines are for extended data. In anti-symmetric extension, the second derivatives are equal to zero at the end boundary points. These points are changed into inflection

Fig. 1 Anti-symmetric end padding method. *Bright lines* are for the extensions



ones because of the original signal extension. Therefore, in 2D wave simulation, the front of adapted points moves smoothly and gradually with constant speed.

The wave propagations are simulated in a string with unit length ($0 \leq x \leq 1$) and unit velocity by anti-symmetric extension method to control the accuracy and stability of numerical simulations in the Dirichlet and Neumann boundary conditions. The simulations are performed by implicit method of lines scheme using two different initial conditions (ICs) and two different boundary conditions (BCs). The assumptions for the simulation of Dirichlet boundary condition (test-1) and Neumann boundary condition (test-2) are as follows, respectively:

$$\text{ICs: } (u(x, t = 0) = 0; \dot{u}(x, t = 0) = 0) \quad \text{and}$$

$$\text{BCs: } u(x = 0, t) = \sin(20\pi \cdot t); u(x = 1, t) = 0,$$

$$\text{ICs: } (u(x, t = 0) = \text{Exp}(-500 \cdot (x - 0.5)^2); \dot{u}(x, t = 0) = 0), \quad \text{and}$$

$$\text{BCs: } (u(x = 0, t) = 0; u'(x = 1, t) = 0).$$

In each test, the exact solution is compared with the results obtained for a specific grid in two different numerical methods. The first method is a conventional scheme that uses one-sided derivatives in its calculation. The second method is based on antisymmetric end padding scheme as described before. To control the convergence of numerical solutions, two different grids, containing 200 and 300 uniform points, are employed in each tests.

In both tests, spatial derivatives are approximated by local Lagrange interpolation method with five points. In the first test to impose boundary condition $u(x = 0, t) = \sin(20\pi \cdot t)$, $u(x = 0, t)$ is differentiated with respect to time. The obtained differential equation is used as an equation in the method of lines scheme. Then, $u(x = 0, t)$ is measured to control the accuracy and stability of solution at the boundary point. In this case, the exact solution at $x = 0$ is $\sin(20\pi \cdot t)$. In the second test, the exact solution [12] is compared with two numerical solutions at $x = 1$. The results of the first test with 200 and 300 grid points are presented in Figs. 2(a) and (b) respectively. The errors ($u_{\text{numerical}} - u_{\text{exact}}$) are computed at $x = 0$. The results of the second test with 200 and 300 grid points are illustrated in Figs. 2(c) and (d), respectively. The errors are calculated at $x = 1$. The results show that the proposed method is comparable with the conventional scheme regarding its accuracy and stability at boundary points. Furthermore, the convergence is improved in the solutions by increasing the number of grid points.

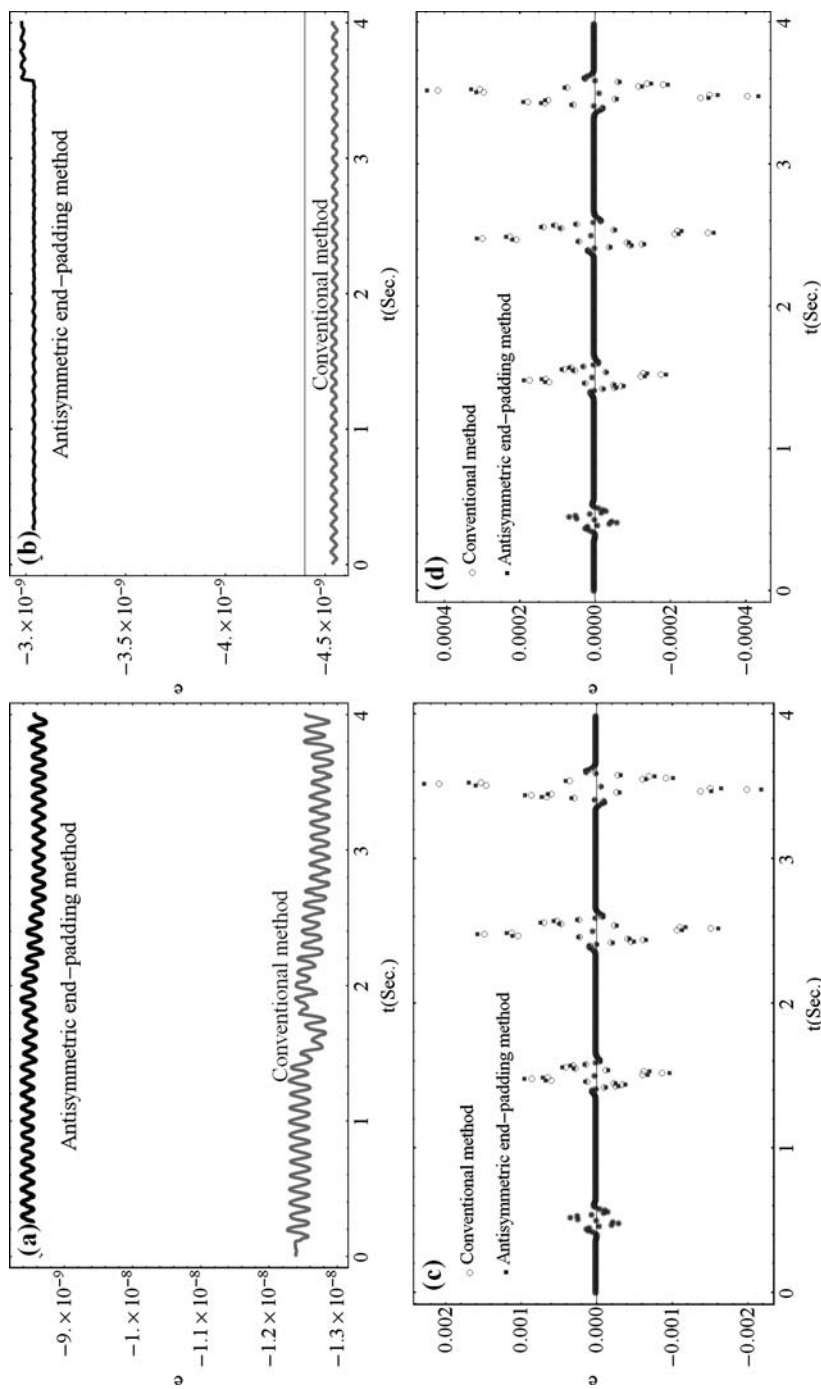


Fig. 2 The accuracy and stability of numerical simulation in the boundary points using conventional (using one-sided derivatives) and anti-symmetric end padding methods as: **(a)**: Dirichlet boundary condition with 200 uniform grid points ($x = 1$). **(b)**: Dirichlet boundary condition with 300 uniform grid points ($x = 0$). **(c)**: Neumann boundary condition with 200 uniform grid points ($x = 1$). **(d)**: Neumann boundary condition with 300 uniform grid points ($x = 1$)

4 Smoothing Splines

The noisy data are recommended not to be fitted exactly, causing significant distortion particularly in the estimation of derivatives. Adaptive solutions, in particular, are sensitive even to small noises (noises may lead to erroneous adapted grid). The smoothing fit is used to remove noisy components in a signal; therefore, interpolation constraint is relaxed. In this research, the spurious oscillations are denoised by smoothing spline directly from the irregular sampled points throughout the solution.

The discrete values of n observations, $y_j = y(x_j)$ where $j = 1, 2, \dots, n$ and $x_1 < x_2 < \dots < x_n$, are assumed in order to determine a smoothing function $f(x)$, that $y_j = f(x_j) + \varepsilon_j$. ε_j are random, uncorrelated errors with zero mean and variance σ_j^2 . Here, $f(x)$ is the smoothest possible function in fitting the observations to a specific tolerance. It is well known that the solution to this problem is the minimizer, $f(x)$, of bellow functional:

$$\lambda \sum_{j=1}^n W_j |y_j - f(x_j)|^2 + \int_{-\infty}^{+\infty} |f^{(m)}(x)|^2 dx, \quad 0 \leq \lambda < +\infty \quad (4.1)$$

where, λ is Lagrangian parameter, W_j is weight factor at point x_j and m is the derivative order.

It can be shown that spline of degree $k = 2m - 1$, having $2m - 2$ continuous derivatives, is an optimal solution for (4.1); where, $n \geq 2m$ [28]. In this paper the cubic smoothing spline is chosen to have a minimum curvature property; hence, $m = 2$ ($2m - 1 = 3$) and $f \in C^2[x_1, x_n]$ [27]. In order to remap the variation range of smoothing parameter (λ) between 0–1, a new parameter (p) is defined as:

$$p = \frac{\lambda}{1 + \lambda}; \quad 0 \leq p \leq 1. \quad (4.2)$$

Then, (4.1) is rewritten as:

$$p \sum_{j=1}^n W_j |y_j - f(x_j)|^2 + (1 - p) \int_{-\infty}^{+\infty} |(d^2 f(x)/dx^2)|^2 dx, \quad 0 \leq p \leq 1. \quad (4.3)$$

According to this formula, the natural cubic spline interpolation is obtained by $p = 1$ and the least-squares straight line fit by $p = 0$. In $p < 1$ the interpolating property is vanished while the smoothing property is increased. In (4.1) and (4.3), the errors are measured by summation and the roughness by integral. Therefore, the smoothness and accuracy are obtained simultaneously. In the mentioned equations, the trade-off between smoothness and goodness of fit to the data is controlled by smoothing parameter. The implementation of smoothing spline is mentioned in [35, 39].

The mentioned new smoothing parameter (p) should be selected properly, otherwise it leads to over-smoothed or under-smoothed results. The former are seen in the scheme presented in [27], according to [15] and the latter in the scheme offered in [5], according to [20].

The smoothness and accuracy in fitting should be incorporated in such a way that the proper adapted grid and accurate solution are obtained simultaneously in adaptive simulations. Hence trial-and-error method is effective in finding appropriate range of p . This study shows that in $\{W_j\} = 1$, the approximated proper values of p are 0.75–0.95. The lower values of p are applicable for non-uniformly weighed data, i.e. $W_j \geq 1$. The values of $\{W_i\}$ and

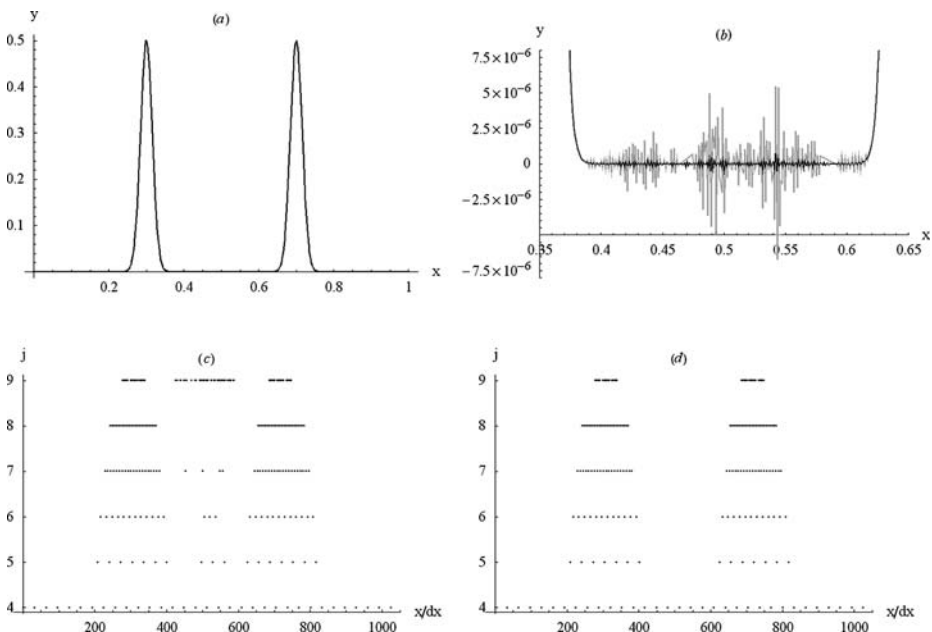


Fig. 3 The effects of smoothing on the solution (a): the solution at 0.2 s; (b): dark line for smoothed solution and light line for numerical solution $p = 0.8$; (c): the adapted points at different levels of resolution before smoothing; (d): the adapted points at different levels of resolution after smoothing

p can be constant or variable for $\{(x_i, y_i)\}$ sequence [21]. Here, the constant weights and smoothing parameter are studied. It is assumed that $\{W_i\} = 1$ in all simulated examples.

A unit length tensioned string is simulated, subjected to the initial imposed deformation, $u_0(x) = \exp(-2000(x - 0.5)^2)$, and the initial velocity, $v_0(x) = 0$. The results are analyzed for the effects of smoothing on the solution accuracy at time $t = 0.2$ s, Fig. 3. In this study, it is assumed that the speed of propagation is 1; i.e. $c = 1$. The numerical solution is obtained in the uniform grid by explicit method of lines scheme, shown in Fig. 3(a). The numerical and corresponding smoothed solutions are compared in Fig. 3(b)—shown in light and dark lines, respectively. The locations of adapted points at different levels of resolution before smoothing are presented in Fig. 3(c) and those of after smoothing in Fig. 3(d). Here, $p = 0.8$ and $\varepsilon = 2 \times 10^{-6}$. The results indicate that some small fluctuations are still remained in the area even after the waves are propagated outwards, Fig. 3(b). These spurious oscillations are mainly concentrated in the finest resolution and could lead to an erroneous adapted grid, Fig. 3(c). However, after smoothing, the proper adaptation is achieved, Fig. 3(d).

Smoothing spline, being less sensitive to noise in the data, has optimal properties for estimating the function and derivatives. The error bounds in estimating the function, belonging to Sobolev space, and its derivatives are presented by Ragozin [26]. He showed that the estimation of function and its corresponding derivatives are converged as the interpolating properties and the sampled points are increased [26]. In the following, the convergence in estimating the function and its corresponding first derivative are studied in L^2 and L_∞ norm senses by selecting a test function. All calculations are carried out by cubic smoothing spline (i.e. $m = 2$). The test function is:

$$f(x) = \sin(2\pi x) + \exp(-\alpha(x - 0.5)^2) \quad (4.4)$$

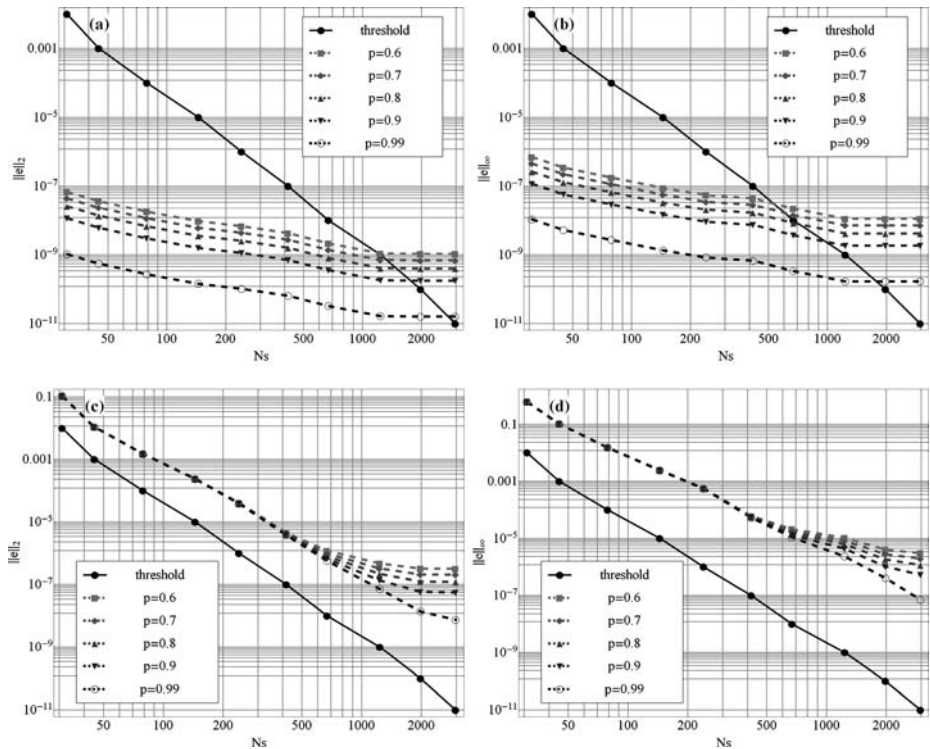


Fig. 4 The errors in the estimations of the test function and its first derivative for different values of smoothing parameter (p). (a), (b): for test function; (c), (d): for its first derivative

where, $\alpha = 10^4$ and $0 \leq x \leq 1$. Here, it is assumed that the $\{W_j\}$ value, used in cubic smoothing spline fitting, is equal to 1 in all calculations; i.e. $\{W_j\} = 1$. The errors in the estimation (energy norm and Sup norm) of test function and its first derivative are shown in Fig. 4. They are plotted against significant points (N_s). These points are obtained by adaptive interpolating wavelet transform (D-D wavelet of order 3) for different p values, 0.99, 0.9, 0.8, 0.7 and 0.6 in all graphs. In energy norm cases, as the number of samples (N_s) and the p values increase, the estimation errors decrease, shown by Ragozin [26]. According to the results, the error curves are nearly parallel in different values of p , especially in the first derivative case. In fact, the denoising effects of smoothing spline and wavelet soft-thresholding (nonlinear smoother) techniques are very similar [34]. Based on the results, the over-smoothing effect is more appeared as p approaches towards zero, especially in the derivative estimation in large values of N_s . In the small values of p , the estimation errors are less sensitive to the N_s of large values, Figs. 4(c) and (d).

5 Numerical Examples

In this section, three Examples 1, 2 and 3 are presented, two of which have smooth solutions with large gradients and the third one is semi-singular. In Examples 1 and 2, two-dimensional elastic wave equations are simulated in finite and infinite domains, respectively.

In Example 3, SH point source is solved in semi-infinite medium. Example 1 has no artificial energy (effective in accuracy decreasing), reflected from boundaries. Therefore, the analysis accuracy is measured studying the different values of smoothing parameter (p). In all examples, D-D wavelet of order 3 is used to adapt grid of solutions.

Example 1 Here, the vibration of a four fixed-sides rectangular membrane, subjected to an initial imposed displacement, is presented. The solution satisfies the following equations:

$$\begin{aligned} \text{PDE} \quad & c_0^2 \left(\frac{\partial^2 u}{\partial x^2} + \frac{\partial^2 u}{\partial y^2} \right) = \frac{\partial^2 u}{\partial t^2}, \quad \Omega \in [0, a] \times [0, b] \quad 0 \leq t < \infty, \\ \text{ICs} \quad & u(x, y, 0) = U(x, y), \quad \dot{u}(x, y, 0) = V(x, y), \\ \text{BCs} \quad & u(0, y, t) = u(1, y, t) = 0, \quad u(x, 0, t) = u(x, 1, t) = 0 \end{aligned} \quad (5.1)$$

where, c_0 is propagation velocity, $U(x, y)$ and $V(x, y)$ are initial imposed displacement and initial imposed velocity, respectively.

The parameters used for the simulations are: $c_0 = 1$, $a = b = 1$, $U(x, y) = \exp(-500(x - 0.5)^2) \cdot \exp(-500(y - 0.5)^2)$, $V(x, y) = 0$, $\varepsilon = 10^{-5}$, $dt = 0.00015$, $p \in \{0.6, 0.7, 0.8, 0.9\}$, $\{W_j\} = 1$ and $m = 3$ (decomposition level). The initial uniform grid has $(2^8 + 1) \times (2^8 + 1)$ points at the finest resolution. Re-adaptation and smoothing are repeated every fifteen time steps.

The numerical solutions are compared with modal analyses. In this regard, the normal modes of rectangular membranes with fixed boundaries are calculated by the bellow formula [12]:

$$m_{nm} = \sin\left(\frac{m\pi x}{a}\right) \cdot \sin\left(\frac{n\pi y}{b}\right). \quad (5.2)$$

The vibration modes are properly superposed and then the modal solution is obtained [12].

The snapshots of adapted grids are prepared at 0.011, 0.389, 0.7807, 0.997, 1.118 and 1.213 s where, $p = 0.8$. They are shown in Fig. 5 in 2 rows and 3 columns, starting from the top left in the first row and following up to the bottom right in the second one. Their correspondent solutions are illustrated in Fig. 6. According to the results, the proper inner and outer moving fronts are formed and the roughly symmetrical adapted grid points are developed before and after reflection.

The results of modal analysis ($n, m \in \{1, 2, \dots, 40\}$) are compared with those of the numerical one for different p values at two receivers. Figures 7(a) and (b) are corresponded to the location (0.5, 0.5) and Figs. 7(c) and (d) to (7/256, 0.5). This comparison is used to study the effects of smoothing on the accuracy of the solutions.

According to the figures, the smaller the values of p , the less the accuracies are and the more apparent the dissipation effects during simulations. The smoothing has such accumulative effect on the errors, Figs. 7(b) and (d), the rate of which increases as p decreases. The spatial adaptive smoothing seems effective in reducing the mentioned drawbacks. In this regard applying non-uniform weight coefficients is recommended, the processes of which will be presented in the future paper.

The numbers of grid points in the simulations, used by adaptation algorithm for different p values, are presented in Fig. 8. Regarding this figure, the smaller the smoothing parameters values, the lower the numbers of needed grid points are.

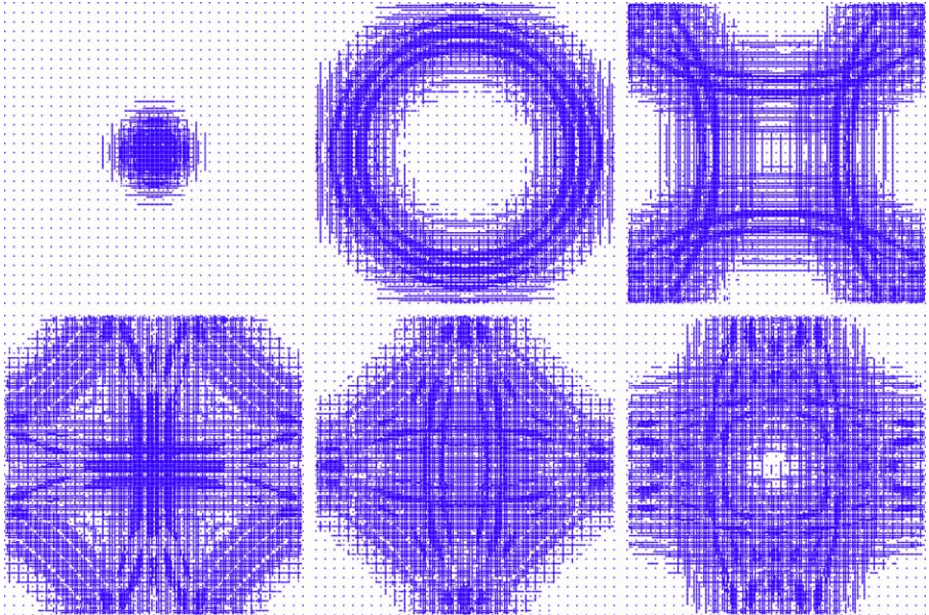


Fig. 5 Snapshots of adapted grids at 0.011, 0.389, 0.7807, 0.997, 1.118 and 1.213 s, starting from the top left snapshot and following the row up to right bottom graph, respectively. $\varepsilon = 10^{-5}$ and $p = 0.8$

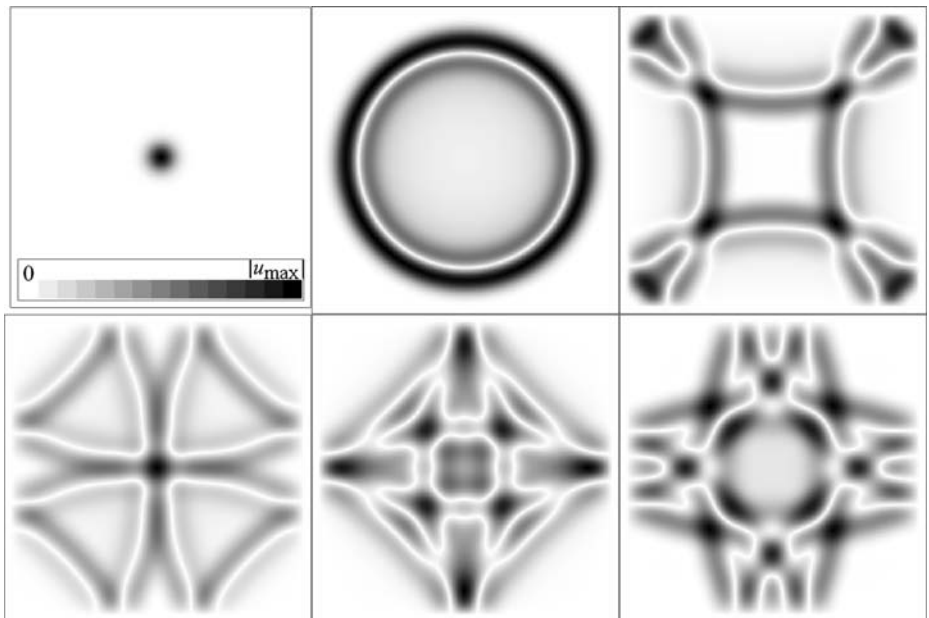


Fig. 6 Snapshots of the solutions at 0.011, 0.389, 0.7807, 0.997, 1.118 and 1.213 s, starting from the top left snapshot and following the row up to right bottom graph, respectively

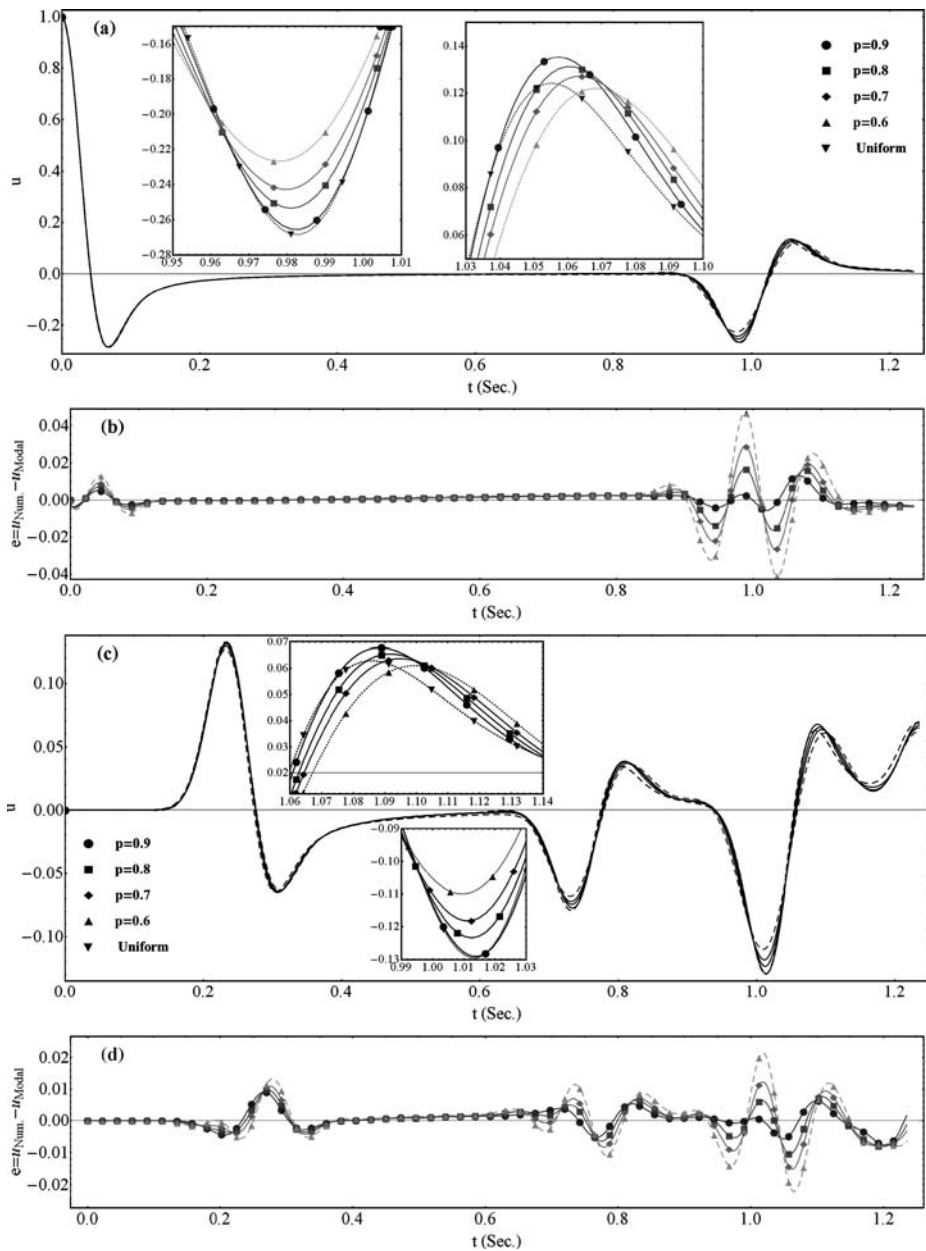


Fig. 7 The solutions and their corresponding errors in modal analysis method and numerical simulation for different p values. (a), (b): for the location (0.5, 0.5); (c), (d): for the location (7/256, 0.5)

Example 2 In this example, an infinite membrane, subjected to the initial imposed deformation, is modeled. The parameters are those of Example 1 except that $\varepsilon = 2 \times 10^{-5}$ and $dt = 0.0003$. Here, the adaptation and smoothing cycles are repeated every ten time steps.

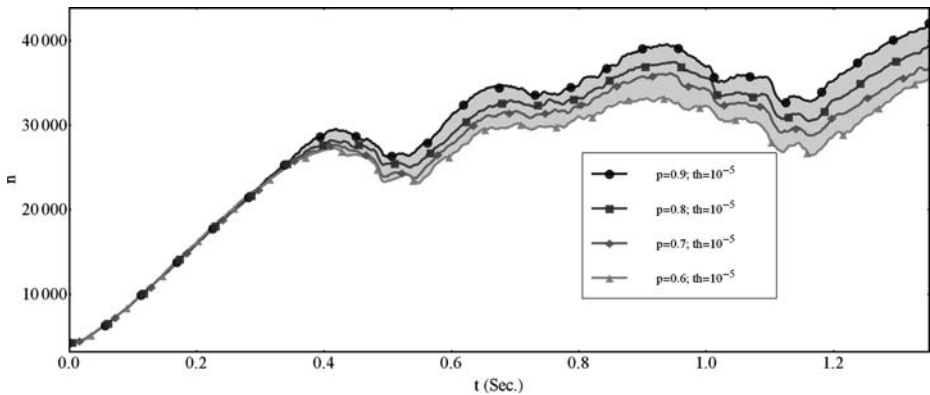


Fig. 8 The grid points used by adaptation algorithm for different values of smoothing parameter (p)

The defect of numerical simulations is occurrence of artificial boundaries which reflect the incoming energies to the computational domain. In this study, the absorbing boundary introduced in [33] is used to simulate infinite boundaries, where the absorbing boundary condition is considered explicitly. Therefore, the wave equation is modified by a damping term $Q(x, y) \cdot \dot{u}(x, y, t)$ where, $Q(x, y)$ is an attenuation factor. This factor is zero in computational domain and increases gradually approaching towards the artificial boundaries. Consequently, the waves incoming towards these boundaries are gradually diminished. In general, no absorbing boundary can dissipate all incoming energies, i.e. some small reflections will always remain.

The modification, explained in the above paragraph, is followed as:

$$\text{PDE} \quad c_0^2 \left(\frac{\partial^2 u}{\partial x^2} + \frac{\partial^2 u}{\partial y^2} \right) = \frac{\partial^2 u}{\partial t^2} + 2Q \frac{\partial u}{\partial t}, \quad \Omega \in [0, 1] \times [0, 1] \quad 0 \leq t < \infty, \quad (5.3)$$

$$\text{ICs} \quad u(x, y, 0) = U(x, y), \quad \dot{u}(x, y, 0) = 0.$$

The factor Q is designed in order to guarantee the gradual reduction of incoming wave energy without reflection. This factor is bounded and twice differentiable with smooth derivatives [33]. Here, Q is considered as:

$$Q(x, y) = a_x (e^{b_x \cdot x^2} + e^{b_x \cdot (1-x)^2}) + a_y (e^{b_y \cdot y^2} + e^{b_y \cdot (1-y)^2}) \quad (5.4)$$

where, $a_x = a_y = 30$ and $b_x = b_y = -80$.

In Fig. 9, the snapshots of adapted grids (top row) and their corresponding solutions (bottom row) are presented at 0.375, 0.591 and 0.735 s in three coupled columns, from left to right, respecting the times. It is obvious that infinite domain is successfully modeled and the proper adapted grids are obtained during the simulation. The exact and numerical solutions [12] are compared at the point (0.5, 0.5), and illustrated in Fig. 10 as solid and dotted lines, respectively. In this figure, the occurrence of a long period reflection from the absorbing boundaries is confirmed.

Example 3 In this example, the point source of SH shear wave is simulated. The numerical model is characterized as: 10 Km both in width and height; the initial uniform grid of 259

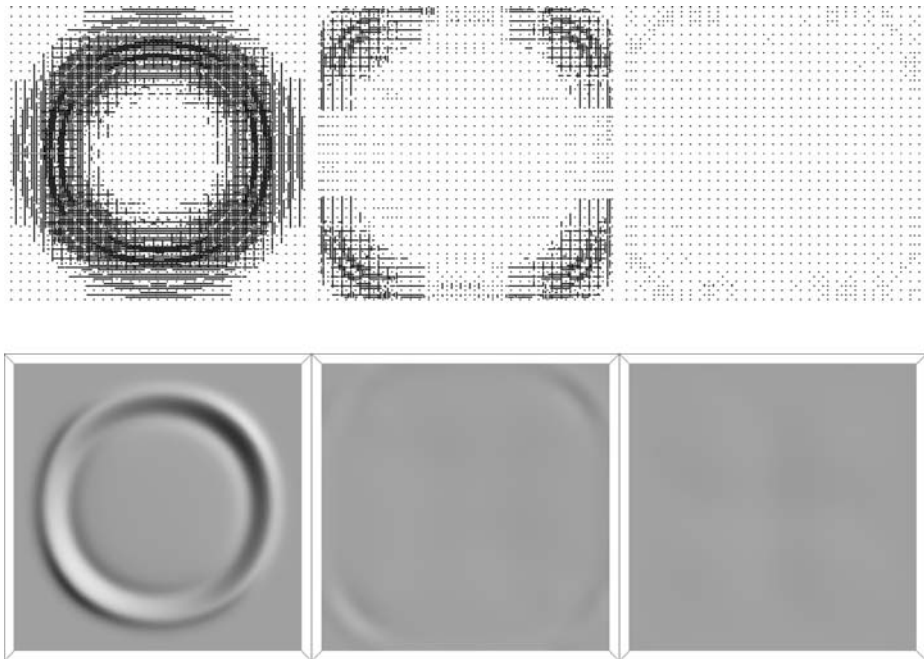


Fig. 9 Snapshots of wave propagation in an infinite media at 0.375, 0.591 and 0.735 s (from left to right, respectively); $\varepsilon = 2 \times 10^{-5}$. The *top row* is for grid points and the *bottom row* is for their corresponding solutions

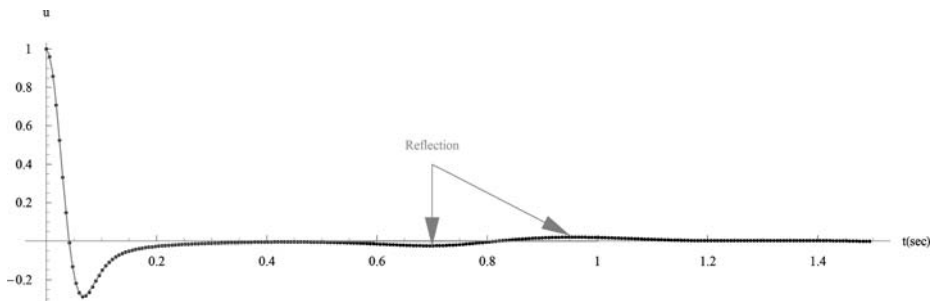


Fig. 10 Comparing the exact (*light solid line*) and numerical (*dotted line*) solutions at point (0.5, 0.5)

by 259; having three absorbing boundaries and one free surface (at the top); the shear wave velocity of $c_0 = 2$ Km/s in the medium of $\rho = 2$ gr/cm³ density. The source is located at 2.77344 Km below the free surface. To monitor responses, three receivers (1, 2 and 3) are located at three points, Fig. 11. The parameters of absorbing boundaries are $a_x = a_y = 30$ and $b_x = b_y = -80$. The factor Q is defined as follows:

$$Q(x, y) = a_x(e^{b_x \cdot (x/10)^2} + e^{b_x \cdot (1-(x/10))^2}) + a_y \cdot e^{b_y \cdot (y/10)^2}. \quad (5.5)$$

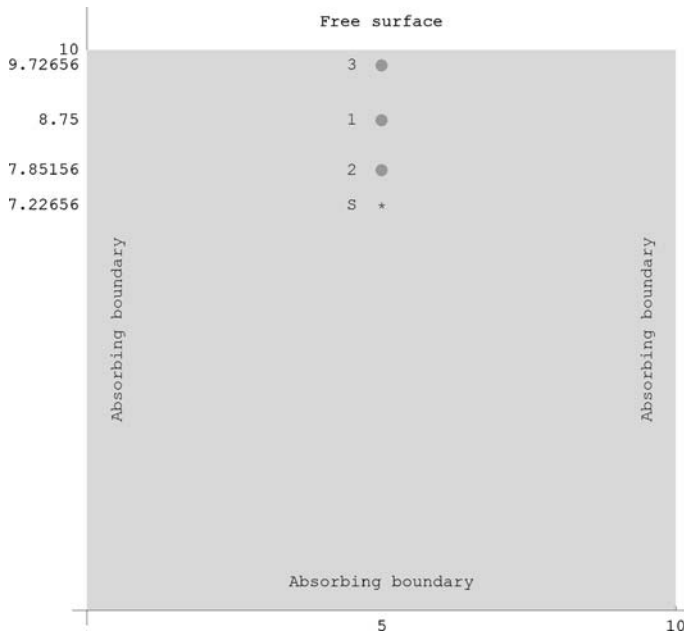


Fig. 11 Semi-infinite domain with free surface. “s” is the position of SH point source and “1”, “2” and “3” are receivers positions

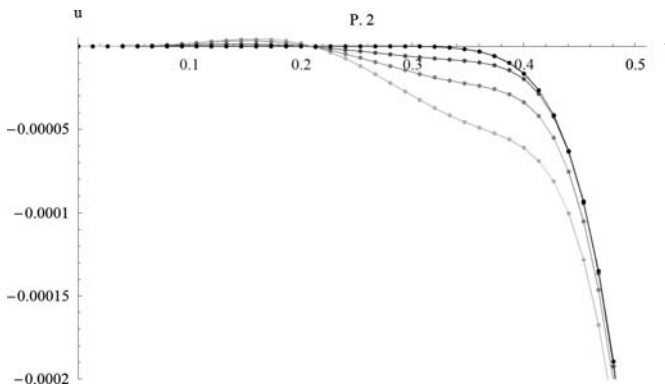


Fig. 12 The effects of threshold values on the accuracy of the solution at the receiver “2”. One exact solution and three numerical solutions (with ε_0 , $2 \times \varepsilon_0$ and $4 \times \varepsilon_0$) dark to light curves, respectively; $\varepsilon_0 = 2.949 \times 10^{-8}$

The source time function $f(t)$ is given by:

$$f(t) = C_s(t - t_0)e^{-\alpha(t-t_0)^2} \quad (5.6)$$

where, $C_s = 15 \times 10^8$, $t_0 = 36$ and $\alpha = 70$.

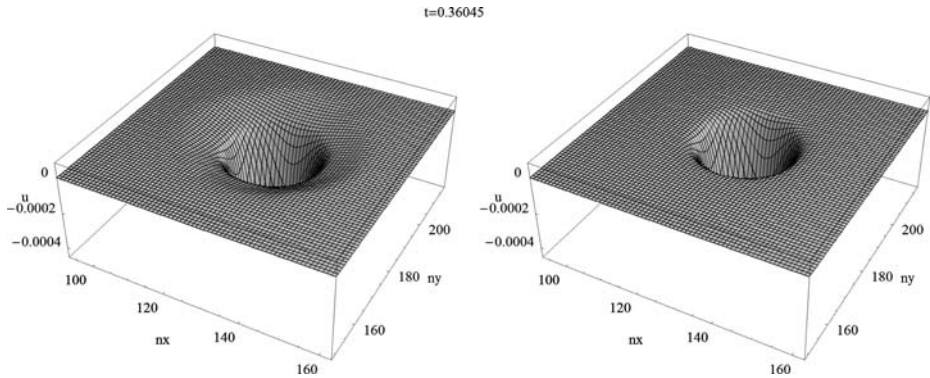


Fig. 13 The effects of threshold on the wave front propagated around the source, ε_0 and $4 \times \varepsilon_0$ right and left figures, respectively

Fig. 14 Time depending threshold

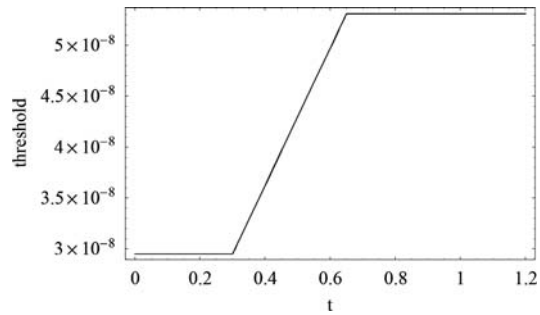
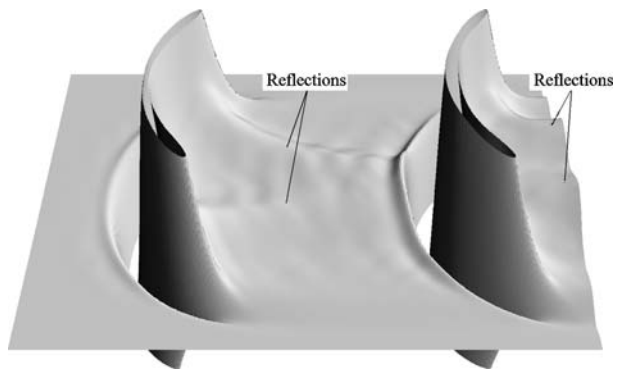


Fig. 15 The reflected waves from absorbing boundaries at time 3.084



The modified equation of SH wave is:

$$\begin{aligned} \text{PDE} \quad c_0^2 \nabla^2 u + \frac{f(t)}{\rho} &= \frac{\partial^2 u}{\partial t^2} + 2Q \frac{\partial u}{\partial t}, \quad \Omega \in [0, 10^4] \times [0, 10^4] \quad 0 \leq t < \infty, \\ \text{ICs} \quad u(x, y, 0) &= 0, \quad \dot{u}(x, y, 0) = 0. \end{aligned} \quad (5.7)$$

The parameters used in this simulation are: $m = 3$ (decomposition level), $p = 0.92$, $dx = 10/2^8$ (Km) and $dt = 0.001335$. Re-adaptation and smoothing processes are repeated every ten time steps.

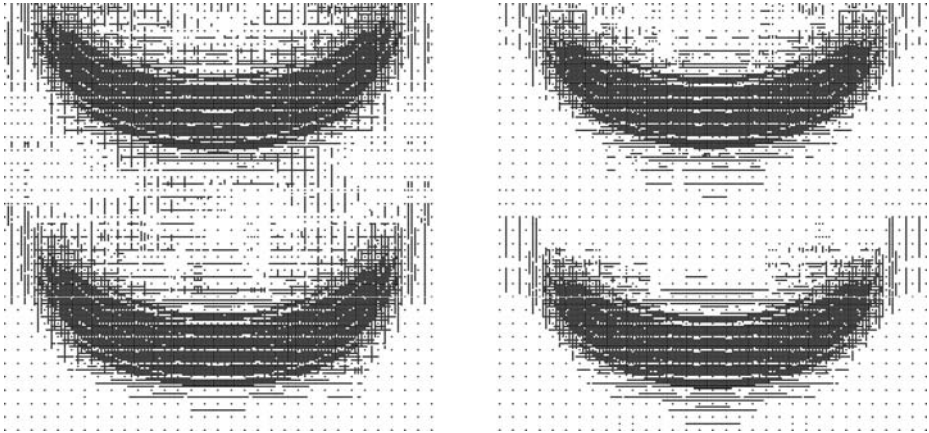


Fig. 16 Two adapted grid points at time 3.084. *Right figure:* for level dependent threshold with $\varepsilon(t)$, $\varepsilon(t)$ and $2 \times \varepsilon(t)$ for levels 7, 6 and 5, respectively. *Left figure:* for non level dependent threshold case, $\varepsilon = \varepsilon(t)$

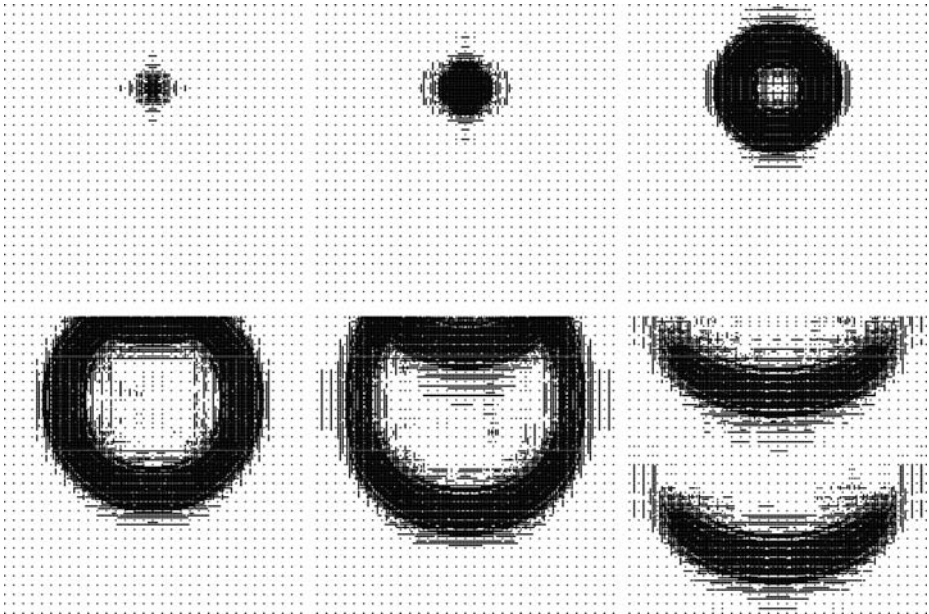


Fig. 17 Snapshots of adapted grids at times 0.04005, 0.46725, 1.10805, 1.90905, 2.28285 and 3.08385 s starting from the top left snapshot and following the row up to right bottom graph, respectively

The effects of threshold on the solution' accuracy is measured at the receiver “2” and presented in Fig. 12. In that figure, in case of $\varepsilon_0 = 2.949 \times 10^{-8}$, the curves of one exact solution and three numerical solutions (with ε_0 , $2 \times \varepsilon_0$ and $4 \times \varepsilon_0$) are shown from dark to light lines, respectively. According to the results, the error levels increase in accordance with the threshold values, causing a drop in the front of propagating waves. The exact solution is obtained by using 2D Green function of infinite elastic homogeneous domain and considering symmetric property [1]. The threshold effects are illustrated by two snapshots

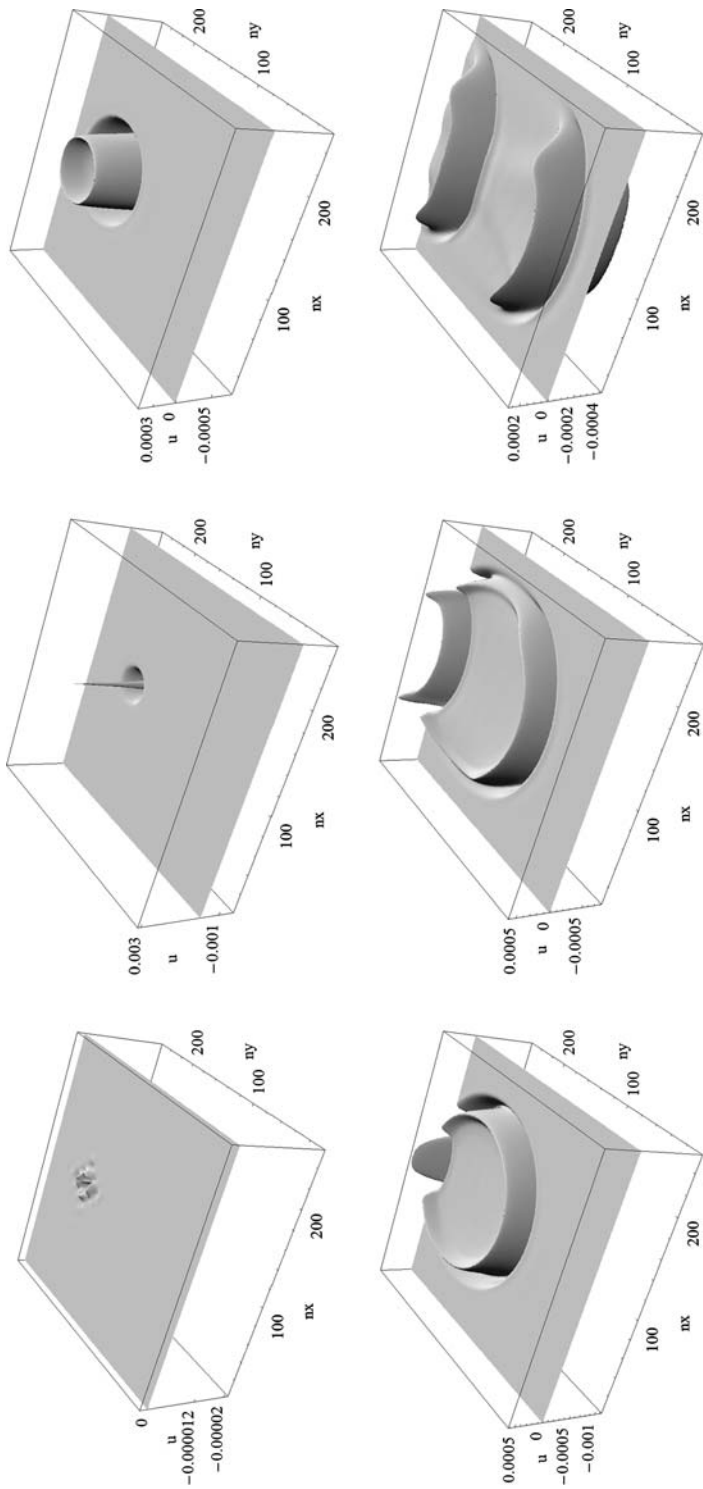


Fig. 18 Snapshots of the solutions at times 0.04005, 0.46725, 1.10805, 1.90905, 2.28285 and 3.08385 s starting from the top left snapshot and following the row up to right bottom graph, respectively

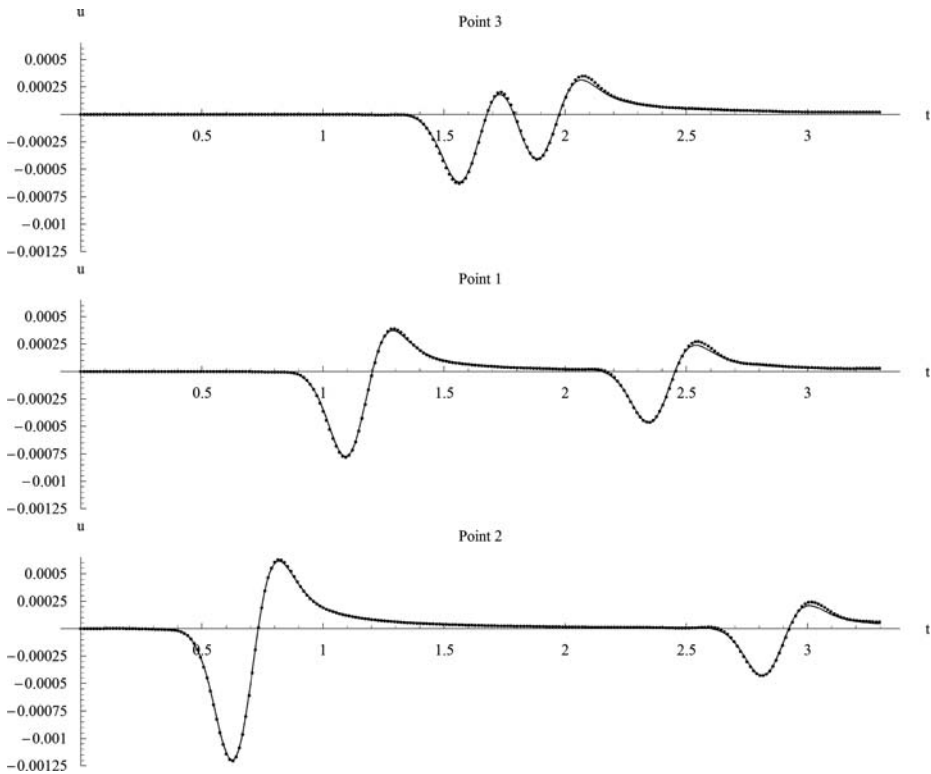
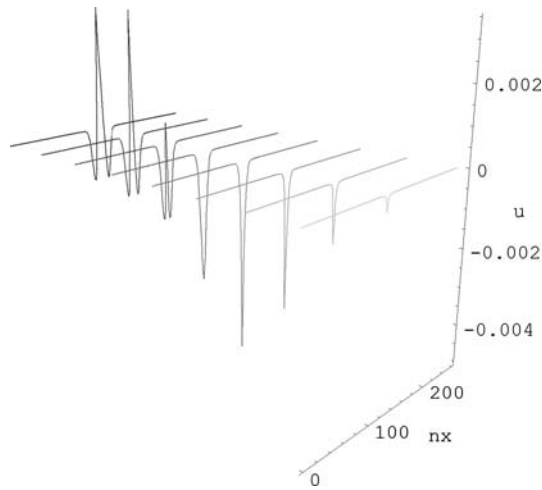


Fig. 19 Comparing the solutions obtained by Green function analysis (*solid line*) and adaptive wavelet-based method (*dotted line*) at points “3”, “1” and “2”

in the vicinity of point source at $t = 0.36045$ s, Fig. 13. Here, the right and left figures are for the thresholds ε_0 and $4 \times \varepsilon_0$, respectively. It is clear that an improper front of propagating wave is produced (left figure) for the threshold of large value. Hence, in this example time-dependent threshold, $\varepsilon(t)$ (Fig. 14) is used for achieving effective and accurate simulations. In this figure the threshold which is ε at initial, it gradually increases to $2 \times \varepsilon$. Therefore, the accuracy of the solution is obtained in the first time steps and the computations are cost effective.

In fact, as all arriving energies are not dissipated by absorbing boundaries, long period waves are reflected and may affect coarse resolutions. The frequency content of propagating waves and the waves correspondingly reflected by absorbing boundaries are higher in this example in comparison with Example 2. These reflected waves may confuse adapted grid points in the coarse resolutions. The reflected waves at time 3.084 s are shown in Fig. 15, the effects of which can be reduced using scale-dependent thresholds, explained earlier in this paper. Therefore, it is assumed that the thresholds of two first fine resolutions (levels 7 and 6) are equal to $\varepsilon(t)$ (Fig. 14) and that of the coarsest resolution (level 5) is $2 \times \varepsilon(t)$. The two adapted grid points are compared at 3.084 s in Fig. 16; the right figure is for the level-dependent thresholding scheme and the left one is for the non level-dependent thresholding method (with $\varepsilon = \varepsilon(t)$). The results show that the reflected waves mainly affect the coarsest resolution with low frequency components.

Fig. 20 Semi-singular solutions around source point at 0.14685, 0.20025, 0.25365, 0.30705, 0.36045, 0.41385, 0.46725 and 0.52065 s from *light to dark* curves, respectively



The adapted grids' snapshots at the 0.04005, 0.46725, 1.10805, 1.90905, 2.28285 and 3.08385 s are shown in Fig. 17 regarding the level and time dependent thresholding frameworks. They are sorted out in two rows and three columns, starting from the top left in the first row and following up to the bottom right in the second one. The correspondent solutions are illustrated in Fig. 18 and ordered as Fig. 17.

The extra noise-like adapted points are observed in the adapted grids in Fig. 17. These points are mainly appeared due to the small non-physical long period waves, reflected by absorbing boundaries. Based on the adapted grid points, the inner and outer propagating fronts are properly obtained before and after the reflection occurred.

The exact solutions, obtained by Green function analysis, and numerical responses are compared at points “3”, “1” and “2”, shown in Fig. 19 from top to bottom, respectively. The results show that the proper solutions are obtained before and after reflections from the free surface. The numerical solutions are measured in the vicinity of source point at 0.14685, 0.20025, 0.25365, 0.30705, 0.36045, 0.41385, 0.46725 and 0.52065 s and presented in Fig. 20, from light to dark curves, respectively. According to the curves, the stable numerical solutions are obtained at the source point despite the existence of semi-singular exact solutions there. In fact, the stable solutions are achieved due to the smoothing of semi-singular solutions.

6 Conclusions

In this research a modified method is presented for adaptive solving second order hyperbolic PDEs, arisen from the wave propagation phenomenon in solid media. The adaptation, the procedure of which is automatically followed during simulation, is achieved by D-D interpolating wavelet of order 3. The smoothing technique is used for reducing the spurious oscillation and the smoothing spline (degree 3) to remove the small non-physical fluctuations. Smoothing splines have many advantages such as: being equipped by fast algorithms, having stability even in ill-posed problems, and estimating smoothly the function and its derivatives. One of the effective and interesting properties of smoothing splines is that they can directly smooth irregular noisy data (the function and its derivatives) and no remapping procedure is needed. Therefore, the calculations are reduced. Furthermore, as all calculations

are performed in physical space, then the proposed method is implemented and understood easily. Finally, to simulate the practical case, time and level-dependent thresholding schemes are used, which may be useful in many situations such as source representation. The proposed method can easily be extended to higher dimensions of PDE and/or system of PDEs. The accuracy of solution can be improved by spatial adaptive smoothing technique. The proposed method in this work is mostly efficient in the numerical simulation of wave-field in the media of localized sharp transition. However, the performance of extended method in the practical simulations, mentioned above, will be reported elsewhere by the authors.

References

1. Achenbach, J.D.: Wave Propagation in Elastic Solids. North-Holland, Amsterdam (1975)
2. Alam, J.M., Kevlahan, N.K.-R., Vasilyev, O.V.: Simultaneous space-time adaptive wavelet solution of nonlinear parabolic differential equations. *J. Comput. Phys.* **214**(2), 829–857 (2006)
3. Bertoluzza, S., Castro, L.: Adaptive wavelet collocation for elasticity: first results. Technical Report 1276, Pub. I.A.N.-C.N.R. de Pavia (2002)
4. Cai, W., Wang, J.: Adaptive multiresolution collocation methods for initial boundary value problems of nonlinear PDEs. *SIAM J. Numer. Anal.* **33**(3), 937–970 (1996)
5. Craven, P., Wahba, G.: Smoothing noisy data with spline functions: estimating the correct degree of smoothing by the method of generalized cross validation. *Numer. Math.* **31**, 377–403 (1979)
6. Cruz, P., Mendes, A., Magalhães, F.D.: Using wavelets for solving PDEs: an adaptive collocation method. *Chem. Eng. Sci.* **56**(10), 3305–3309 (2001)
7. Cruz, P., Mendes, A., Magalhães, F.D.: Wavelet-based adaptive grid method for the resolution of nonlinear PDEs. *AIChE J.* **48**(4), 774–785 (2002)
8. Donoho, D.L.: Interpolating wavelet transforms. Technical Report 408, Dept. of Statistics, Stanford University, Stanford (1992)
9. Fatkullin, I., Hesthaven, J.S.: Adaptive high-order finite-difference method for nonlinear wave problems. *J. Sci. Comput.* **16**(1), 47–67 (2001)
10. Fornberg, B.: Calculation of weights in finite difference formulas. *SIAM Rev.* **40**(3), 685–691 (1998)
11. Gottlieb, D., Hesthaven, J.S.: Spectral methods for hyperbolic problems. *J. Comput. Appl. Math.* **128**(1–2), 83–131 (2001)
12. Graff, K.F.: Wave Motion in Elastic Solids. Dover, New York (1973)
13. Holmström, M.: Solving hyperbolic PDEs using interpolating wavelets. *SIAM J. Sci. Comput.* **21**(2), 405–420 (1999)
14. Holmström, M., Waldén, J.: Adaptive wavelet methods for hyperbolic PDEs. *J. Sci. Comput.* **13**(1), 19–49 (1998)
15. Hutchinson, M.F., de Hoog, F.R.: Smoothing noisy data with spline functions. *Numer. Math.* **47**(1), 99–106 (1985)
16. Jameson, L.M.: A wavelet-optimized, very high order adaptive grid and order numerical method. *SIAM J. Sci. Comput.* **19**(6), 1980–2013 (1998)
17. Jameson, L.M., Miyama, T.: Wavelet analysis and ocean modeling: a dynamically adaptive numerical method “WOFD-AHO”. *Mon. Weather Rev.* **128**(5), 1536–1548 (2000)
18. Jansen, M.: Noise Reduction by Wavelet Thresholding. Lecture Notes in Statistics, vol. 161. Springer, New York (2001)
19. Kevlahan, N.K.-R., Vasilyev, O.V.: An adaptive wavelet collocation method for fluid-structure interaction at high Reynolds numbers. *SIAM J. Sci. Comput.* **26**(6), 1894–1915 (2005)
20. Lee, T.C.M.: Smoothing parameter selection for smoothing splines: a simulation study. *Comput. Stat. Data Anal.* **42**(1–2), 139–148 (2003)
21. Lee, T.C.M.: Improved smoothing spline regression by combining estimates of different smoothness. *Stat. Probab. Lett.* **67**(2), 133–140 (2004)
22. Liu, Y., Cameron, I.T., Wang, F.Y.: The wavelet collocation method for transient problems with steep gradients. *Chem. Eng. Sci.* **55**(9), 1729–1734 (2000)
23. Loader, C.: Smoothing: local regression techniques. In: Gentle, J.E., Härdle, W., Mori, Y. (eds.) *Handbook of Computational Statistics Concepts and Methods*, pp. 539–564. Springer, Berlin (2004)
24. Mallet, S.: A Wavelet Tour of Signal Processing. Academic Press, San Diego (1998)
25. Nievergelt, Y.: Wavelets Made Easy. Birkhauser, Boston (1999)
26. Ragozin, D.L.: Error bounds for derivative estimates based on spline smoothing of exact or noisy data. *J. Approx. Theory* **37**, 335–355 (1983)

27. Reinsch, C.H.: Smoothing by spline functions. *Numer. Math.* **10**, 177–183 (1967)
28. Reinsch, C.H.: Smoothing by spline functions, II. *Numer. Math.* **16**, 451–454 (1971)
29. Salomon, D.: *Curves and Surfaces for Computer Graphics*. Springer, New York (2006)
30. Santos, J.C., Cruz, P., Magalhães, F.D., Mendes, A.: 2D wavelet-based adaptive grid method for the resolution of PDEs. *AICHE J.* **49**(3), 706–717 (2003)
31. Santos, J.C., Cruz, P., Alves, M.A., Oliveira, P.J., Magalhães, F.D., Mendes, A.: Adaptive multiresolution approach for two-dimensional PDEs. *Comput. Methods Appl. Mech. Eng.* **193**(3), 405–425 (2004)
32. Shi, Z., Kouri, D.J., Wei, G.W., Hoffman, D.K.: Generalized symmetric interpolation wavelets. *Comput. Phys. Commun.* **119**(2–3), 194–218 (1999)
33. Sochacki, J., Kubichek, R., George, J., Fletcher, W.R., Smithson, S.: Absorbing boundary conditions and surface waves. *Geophysics* **52**(1), 60–71 (1987)
34. Unser, M.: Splines: a perfect fit for signal/image processing. *IEEE Signal Process. Mag.* **16**(6), 22–38 (1999)
35. van den Bogert, T.: Practical guide to smoothing and filtering. Available from Netlib. <http://isb.ri.ccf.org/isb/software/bogert/filter.ps> (1996)
36. Vasilyev, O.V., Kevlahan, N.K.-R.: An adaptive multilevel wavelet collocation method for elliptic problems. *J. Comput. Phys.* **206**(2), 412–431 (2005)
37. Vasilyev, O.V., Paolucci, S.: A dynamically adaptive multilevel wavelet collocation method for solving partial differential equations in a finite domain. *J. Comput. Phys.* **125**(2), 498–512 (1996)
38. Vasilyev, O.V., Paolucci, S.: A fast adaptive wavelet collocation algorithm for multidimensional PDEs. *J. Comput. Phys.* **138**(1), 16–56 (1997)
39. Woltring, H.J.: A FORTRAN package for generalized, cross validatory spline smoothing and differentiation. *Adv. Eng. Softw.* **8**(2), 104–113 (1986)